


# Biogeochemical changes at the sediment–water interface during redox transitions in an acidic reservoir: exchange of protons, acidity and electron donors and acceptors

A. Corzo  · J. L. Jiménez-Arias · E. Torres · E. García-Robledo · M. Lara · S. Papaspyrou

Received: 31 January 2018 / Accepted: 28 June 2018 / Published online: 5 July 2018  
© The Author(s) 2018

**Abstract** Redox transitions induced by seasonal changes in water column O<sub>2</sub> concentration can have important effects on solutes exchange across the sediment–water interface in systems polluted with acid mine drainage (AMD), thus influencing natural attenuation and bioremediation processes. The effect of such transitions was studied in a mesocosm experiment with water and sediment cores from an acidic reservoir (El Sancho, SW Spain). Rates of aerobic organic matter mineralization and oxidation of

reduced inorganic compounds increased under oxic conditions (OX). Anaerobic process, like Fe(III) and sulfate reduction, also increased due to higher O<sub>2</sub> availability and penetration depth in the sediment, resulting in higher regeneration rates of their corresponding anaerobic e<sup>-</sup> acceptors. The contribution of the different processes to oxygen uptake changed considerably over time. pH decreased due to the precipitation of schwertmannite and the release of H<sup>+</sup> from the sediment, favouring the dissolution of Al-hydroxides and hydroxysulfates at the sediment surface. The increase in dissolved Al was the main contributor to water column acidity during OX. Changes in organic matter degradation rates and co-precipitation and dissolution of dissolved organic carbon and nitrogen with redox-sensitive Fe(III)

---

Responsible Editor: Jennifer Leah Tank.

**Electronic supplementary material** The online version of this article (<https://doi.org/10.1007/s10533-018-0465-7>) contains supplementary material, which is available to authorized users.

---

A. Corzo (✉) · J. L. Jiménez-Arias · E. García-Robledo · M. Lara · S. Papaspyrou  
Departamento de Biología, Facultad de Ciencias del Mar y Ambientales, Universidad de Cádiz, Pol. Río San Pedro s/n, 11510 Puerto Real, Cádiz, Spain  
e-mail: alfonso.corzo@uca.es

E. Torres  
Instituto de Diagnóstico Ambiental y Estudios del Agua (IDAEA), CSIC, Jordi Girona, 18-26, 08034 Barcelona, Spain

S. Papaspyrou  
Unidad Asociada de Oceanografía Interdisciplinar, Instituto de Ciencias Marinas de Andalucía (CSIC), Avenida República Saharaui s/n, 11510 Puerto Real, Spain

*Present Address:*  
S. Papaspyrou  
Área de Microbiología, Department of Biomedicine, Biotechnology and Public Health, University of Cadiz, Spain, Pol. Río San Pedro s/n, 11510 Puerto Real, Cádiz, Spain

compounds affected considerably C and N cycling at the sediment–water interface during redox transitions. The release of  $\text{NO}_2^-$  and  $\text{NO}_3^-$  during the hypoxic period could be attributed to ammonium oxidation coupled to ferric iron reduction (Feammox). Considering the multiple effects of redox transitions at the sediment–water interface is critical for the successful outcome of natural attenuation and bioremediation of AMD impacted aquatic environments.

**Keywords** Acid mine drainage · Lake · Microscale · Microsensor · Oxic-anoxic interface · Acidity · Iron · Sulfur · Fluxes at the sediment–water interface · Diffusive oxygen uptake · Carbon mineralisation calculations · Huelva · Iberian pyrite belt · Sancho reservoir

## Introduction

Acid mine drainage (AMD) is the result of the oxidation of sulfide minerals exposed to the atmosphere as a side effect of mining. This oxidation is mediated by a combination of abiotic and microbial reactions and produces waters with a very low pH and high concentrations of  $\text{SO}_4^{2-}$ , Fe, and other metals and metalloids. AMD causes high environmental impact, producing serious and long-persisting problems for ecosystem functioning and human health (Geller et al. 2009). Enhancing natural neutralization by favoring microbial and biogeochemical processes that consume acidity and increase the pH is one of the most promising approaches to treat AMD effluents and restore affected ecosystems (Geller et al. 2009; Koschorreck et al. 2007a). However, seasonal changes in the  $\text{O}_2$  availability and pH affect the long term success and reversibility of such bioremediation approaches in acid lakes and reservoirs (Geller et al. 2009).

Oxygen availability affects microbial metabolism, organic matter mineralization pathways and numerous abiotic redox-dependent physicochemical and mineralogical processes (Froelich et al. 1978; Torres et al. 2014). Under oxic conditions, aerobic oxidation of organic matter (Table 1; R1), abiotic and biological oxidation of  $\text{H}_2\text{S}$  and Fe(II) by  $\text{O}_2$  (Table 1; R5 and R6), and the precipitation of Fe(III) oxyhydroxides (Table 1; R12) contribute to lowering the pH

(Jourabchi et al. 2005; Soetaert et al. 2007). In contrast, under anoxic conditions, organic matter is mineralized anaerobically by bacteria utilizing an array of electron acceptors (e.g.  $\text{SO}_4^{2-}$ , Fe(III),  $\text{NO}_3^-$ ) (Table 1; R2, R4 and R3) which consume  $\text{H}^+$ , leading to an increase in pH during stratification (Jourabchi et al. 2005; Soetaert et al. 2007). Therefore, redox transitions, through the changes in  $\text{O}_2$  availability and pH, can potentially affect many different biogeochemical processes in aquatic environments, which in turn determine the fluxes between the sediment and water column and the mobility of elements, nutrients and contaminants within the sediment. Changes in chemical speciation, bioavailability, toxicity and mobility of many metal and non-metal elements (Borch et al. 2010), bioavailability of limiting nutrients like phosphate (Gunnars and Blomqvist 1997; Hupfer and Lewandowski 2008), and the concentration, speciation and susceptibility to degradation of dissolved organic matter (Sinninghe Damste and De Leeuw 1990; Zonneveld et al. 2010; Arndt et al. 2013) are a few examples of the impact of redox transitions on key processes of aquatic ecosystems. Most likely many other effects remain unknown or poorly studied. In addition, redox oscillations also affect the microbial community (Frindte et al. 2013, 2016).

The effect of hypolimnetic hypoxic and anoxic conditions on degradation and preservation rates of organic matter and the regeneration and release of nutrients from lake sediments has received considerable attention (Maerki et al. 2009; Matzinger et al. 2010; Schwefel et al. 2017). However, the number of studies dealing specifically with the effects of reversible redox oscillations on the biogeochemistry of lake sediments is scarce (Borch et al. 2010; Frindte et al. 2013; Torres et al. 2014; Karimian et al. 2017). More specifically, the effect of redox transitions on spatiotemporal changes of key variables like  $\text{O}_2$  and pH and their interaction with the biogeochemical cycling of C, Fe, and S at the sediment–water interface have rarely been investigated simultaneously (Elberling and Damgaard 2001, Koschorreck et al. 2003, 2007a). This information is critical to understand and model net fluxes of inorganic nutrients, electron donors and acceptors, metal and non-metal elements, and organic compounds between the sediment and the water column. We hypothesized that redox transitions change the availability and micro-scale distribution of relevant electron donor and

**Table 1** Major primary and secondary redox and mineral precipitation-dissolution reactions considered in the Sancho Reservoir sediment–water system

Reaction	Reaction and stoichiometry
1. Aerobic respiration	$\text{CH}_2\text{O} + \text{O}_2 \rightarrow \text{HCO}_3^- + \text{H}^+$
2. Sulfate reduction	$2\text{CH}_2\text{O} + \text{SO}_4^{2-} \rightarrow \text{H}_2\text{S} + 2\text{HCO}_3^-$
3. Nitrate reduction	$\text{CH}_2\text{O} + \text{NO}_3^- + 2\text{H}^+ \rightarrow \text{CO}_2 + \frac{1}{2}\text{N}_2 + 2\text{H}_2\text{O}$
4. Iron reduction	$\frac{1}{4}\text{CH}_2\text{O} + \text{FeOOH}_{(s)} + \frac{7}{4}\text{H}^+ \rightarrow \text{Fe}^{2+} + \frac{1}{4}\text{HCO}_3^- + \frac{3}{2}\text{H}_2\text{O}$
5. Sulfide oxidation by $\text{O}_2$	$\text{H}_2\text{S} + 2\text{O}_2 \rightarrow \text{SO}_4^{2-} + 2\text{H}^+$
6. Iron oxidation by $\text{O}_2$	$\text{Fe}^{2+} + \frac{1}{4}\text{O}_2 + \text{H}^+ \rightarrow \text{Fe}^{3+} + \frac{1}{2}\text{H}_2\text{O}$
7. Sulfide oxidation by $\text{Fe}^{3+}$	$\frac{1}{8}\text{H}_2\text{S} + \text{FeOOH}_{(s)} + \frac{7}{4}\text{H}^+ \rightarrow \text{Fe}^{2+} + \frac{1}{8}\text{SO}_4^{2-} + \frac{3}{2}\text{H}_2\text{O}$
8. Metal sulfide precipitation ( $\text{M} = \text{Fe}^{2+}, \text{Cu}^{2+}, \text{Zn}^{2+}, \text{Ni}^{2+}$ or $\text{Co}^{2+}$ )	$\text{M}^{2+} + \text{H}_2\text{S} \rightarrow \text{MS}_{(s)} + 2\text{H}^+$
9. Pyrite formation	$\text{FeS}_{(s)} + \text{H}_2\text{S} \rightarrow \text{FeS}_{2(s)} + \text{H}_2$
10. Metal sulfide oxidation by $\text{O}_2$ ( $\text{M} = \text{Fe}^{2+}, \text{Cu}^{2+}, \text{Zn}^{2+}, \text{Ni}^{2+}$ or $\text{Co}^{2+}$ )	$\text{MS}_{x(s)} + \frac{3}{2}x\text{O}_2 + x\text{H}_2\text{O} \rightarrow \text{M}^{2+} + x\text{SO}_4^{2-} + 2x\text{H}^+$
11. OM sulfidization	$\text{OM} + \text{H}_2\text{S} \rightarrow \text{OM} - \text{H}_2\text{S}$
12. Schwertmannite precipitation	$8\text{Fe}^{3+} + \text{SO}_4^{2-} + 14\text{H}_2\text{O} \rightarrow \text{Fe}_8\text{O}_8(\text{OH})_6\text{SO}_4 + 22\text{H}^+$
13. Hydrobasaluminite precipitation	$4\text{Al}^{3+} + \text{SO}_4^{2-} + 22 - 46\text{H}_2\text{O} \rightarrow \text{Al}_4(\text{SO}_4)(\text{OH})_{10}12 - 36\text{H}_2\text{O} + 10\text{H}^+$

acceptors at the sediment water interface, which ultimately determine the rates and pathways of processes that affect pH and acidity in acidic environments such as organic matter mineralization and the net exchange of iron and aluminium.

The aim of this study was to determine how the hypoxic-oxic and oxic-hypoxic transitions affect the microscale distribution within the sediment and biogeochemical fluxes across the sediment–water interface of the most important electron donors and acceptors, protons, acidity and organic and inorganic nutrients in a model AMD contaminated environment. These redox transitions were studied in a mesocosm experiment with water and sediment cores from the Sancho Reservoir (Iberian Pyrite Belt, SW Spain). Relevant biogeochemical variables ( $\text{O}_2$ ,  $\text{H}_2\text{S}$ ,  $\text{H}^+$ , inorganic N, Fe, Al, acidity, dissolved organic carbon and nitrogen) were monitored at different spatiotemporal scales in the water column, pore water and sediment solid phases. Based on this experiment, Torres et al. (2014) constructed and calibrated a diffusion–reaction model to calculate the net fluxes of metals, taking into account the annual variation of oxic and anoxic conditions of the bottom water, and to predict overall water quality. Here, we focus on the interaction between the cycles of several important

elements (organic carbon, nitrogen, oxygen, sulfur, iron and aluminium) and their effect on the exchange of  $\text{H}^+$ , acidity and  $e^-$  donors and acceptors across the sediment–water interface. The detailed study of redox transitions at the sediment–water interface is not only of theoretical interest but also of a practical one, since it advances our understanding of the biogeochemical and microbial processes behind the immobilization within the sediment or release to the water column of elements affecting the natural neutralization. This is important to increase our predictive capacity on the potential long-term success of current bioremediation ecotechnological treatments.

## Materials and methods

### Study site, cores and bottom water collection

The Sancho Reservoir ( $37^\circ 27' \text{N}$ ,  $6^\circ 59' \text{O}$ ) is located on the Odiel River catchment (Southwest Spain). The reservoir ( $58 \text{ Hm}^3$ ,  $42.7 \times 10^5 \text{ m}^2$  and a maximum depth of 40 m close to the dam), with a pH around 3.5, is affected by the discharge of the Meca River. This river is heavily contaminated by AMD, with high concentrations of trace metals, iron and  $\text{SO}_4^{2-}$ , and a

mean pH of 2.6 (Sarmiento et al. 2009; Cánovas et al. 2016). The Sancho Reservoir is a warm monomictic body of water. During winter, the entire water column is mixed and dissolved oxygen reaches the sediment. During the rest of the year, the water column is stratified and anoxic conditions develop below 15 m (Torres et al. 2013, 2016).

Twelve sediment cores (5.8 cm internal diameter, 60 cm length) were collected using a gravity corer (UWITEC) from a depth of about 30 m close to reservoir dam during the stratification period (November 15th, 2010). The collected cores had around 30 cm of sediment and 30 cm of overlying bottom water. In situ temperature,  $O_2$ , and pH, measured with a multiparameter probe (Hydrolab MS5), showed characteristic profiles of a late stratification phase (data not

shown). Anoxic bottom water was collected with a Niskin bottle approximately 1.5 m above the sediment surface from the same sampling site. Cores and bottom water were protected from light and stored on ice (4 °C) until return to the laboratory on the same day (within 5 h).

### Experimental design

In the laboratory, all cores were introduced in a temperature controlled (12–14 °C) tank filled with 25 L of in situ bottom water. Cores were maintained in the dark under hypoxic or oxic conditions as described below. Hypoxic conditions ( $24 \mu\text{mol } O_2 \text{ L}^{-1}$ , < 8% saturation) were obtained by vigorous bubbling of the tank water with  $N_2$ . Although the initial objective was

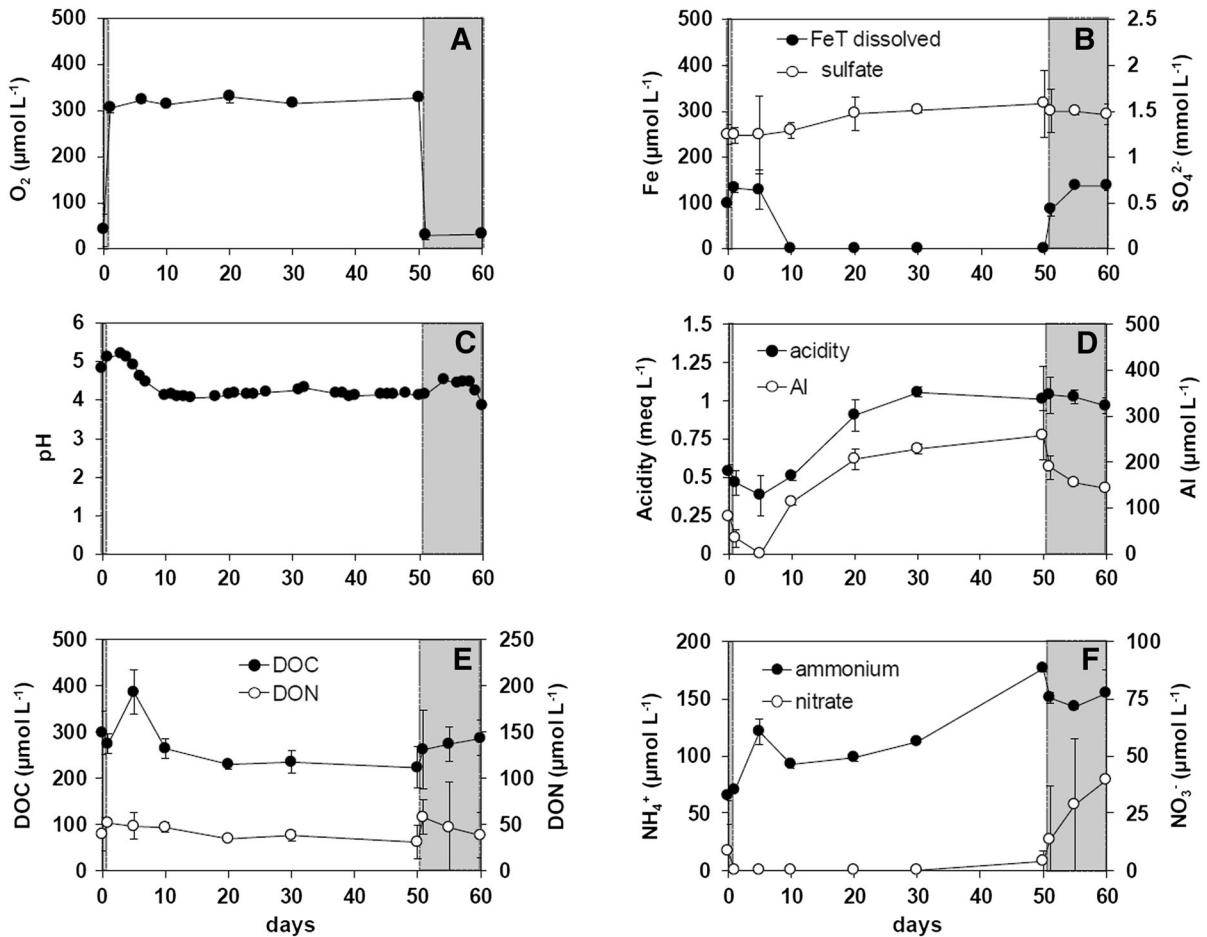


**Fig. 1** Temporal evolution of  $O_2$ , Fe,  $SO_4^{2-}$ , pH, acidity, Al, dissolved organic carbon (DOC), dissolved organic nitrogen (DON),  $NH_4^+$  and  $NO_3^-$  in the bulk water phase during the

experiment. Data are presented as mean  $\pm$  standard error ( $n = 3$ ). Areas shaded in grey indicated initial and final hypoxic conditions periods

to obtain the same anoxic conditions as observed in situ, we were unable to reduce the  $O_2$  concentration to zero in a system open to the laboratory atmosphere. Microsensor measurements also required an open system to allow measurements across the sediment–water interface as described below.

The experiment was divided in three different stages: (1) initial hypoxic stage (HI), maintained with a  $N_2$  flux during 1 day, (2) oxic stage (OX), where the conditions of the water in the tank were switched to oxic by bubbling air into the tank, and maintained during 50 days, (3) final hypoxic stage (HF), which lasted 10 days, induced by bubbling  $N_2$  in the tank. A more detailed description and a sketch of the experimental design can be found elsewhere (Torres et al. 2014).

#### Water column and sediment analyses

Oxygen (oxygen electrode Crison OXI 45 P), pH, and temperature (pH electrode, Orion) of the bulk water phase of the tank were monitored during the whole experiment. Water from the tank was sampled on days 0, 1, 5, 10, 20, 30, 50, 51, 55 and 60. Water level was constant during stages 1 and 2. A slight evaporation was produced by the dry  $N_2$  bubbling during stage 3, and the solute concentrations were corrected assuming Mg conservative. Water samples were filtered through 0.2  $\mu\text{m}$  nylon filters, acidified with 20%  $HNO_3$  (final  $\text{pH} < 2$ ) and stored in darkness at  $-20^\circ\text{C}$  until analysis. Dissolved organic carbon (DOC) and dissolved total nitrogen (DTN) were measured on a TOC-Analyser (Thermo Finnigan, FlashEA1112) with an analytical error of 1.5 and 3%, respectively. Ammonium (detection limit: 2.38  $\mu\text{M}$ ) was analyzed according to Bower and Holm-Hansen (1980), and nitrate (detection limit: 2.15  $\mu\text{M}$ ) and nitrite (detection limit: 0.24  $\mu\text{M}$ ) were analyzed according to García-Robledo et al. (2014). Dissolved organic nitrogen (DON) was calculated as the difference between DTN and total dissolved inorganic nitrogen ( $\text{NO}_3^- + \text{NO}_2^- + \text{NH}_4^+$ ). Phosphate (detection limit: 2.38  $\mu\text{M}$ ) was measured according to Grasshoff (1983) and total P (detection limit: 0.2  $\text{mg L}^{-1}$ ) by ICP-AES.

At the end of each stage, three cores were removed from the tank and processed for geochemical analyses of the sediment solid phase and pore water. Cores were sliced in several layers, 1-cm slices for the first 8 cm, and 2-cm slices down to 16 cm depth, inside a  $N_2$ —

purged glove box. Total organic carbon ( $C_{\text{org}}$ ) was measured on a Thermo EA1108 elemental organic analyzer using standard protocols. Total nitrogen and total sulfur contents were measured on a CNHS elemental analyzer (Thermo EA Flash 2000) using standard protocols. The analytical error for  $C_{\text{org}}$ , N and S was below 5%. Pore water was extracted from every layer by centrifugation, filtered through 0.2  $\mu\text{m}$  nylon filters. S, Al, Fe, and other metals were analyzed by inductively coupled plasma atomic emission spectrometry (ICP-AES) using a Thermo Jarrel-Ash instrument equipped with a CID detector (analytical error 6%). Fe in solution was always considered to be in the form of ferrous iron ( $\text{Fe}^{2+}$ ) since the pH was generally higher than 4 in the pore water and the water column (Stumm and Morgan 1996). Sulfate was calculated from total S assuming that other intermediate aqueous S species were of minor abundance compared to  $\text{SO}_4^{2-}$  in our experimental conditions (Smith and Melville 2004; Torres et al. 2014).

Acidity was estimated from metal and  $H^+$  concentrations, as usually considered in AMD environments (Kirby and Cravotta 2005), according to Eq. (1).

$$\begin{aligned} \text{Acidity} = & 3(c_{\text{Al}} + c_{\text{Fe(III)}}) \\ & + 2(c_{\text{Fe(II)}} + c_{\text{Mn}} + c_{\text{Zn}} + c_{\text{Cu}} + c_{\text{Ni}} + c_{\text{Co}}) \\ & + 10^{-\text{pH}} \end{aligned} \quad (1)$$

where  $c_x$  are molal concentrations of element x.

#### Microsensor measurements

Vertical distributions of  $O_2$ , pH, and  $H_2S$  were determined at the sediment–water interface using selective microelectrodes after 1 day under HI conditions, and on days 1, 6, 10, 20, and 50 (OX stage), and days 51, 56, and 60 (HF stage) in the same 3 cores during the three stages of the experiment. On each sampling occasion, one core at a time was removed from the tank and maintained under a continuous flow-through system with in situ bottom water at similar physicochemical conditions (T,  $O_2$ , pH) than those of the tank for the duration of the measurements ( $\sim 1$  h). Microelectrodes (Unisense<sup>®</sup>, Denmark) were used and calibrated according to Unisense manuals ([www.unisense.com](http://www.unisense.com)) and as described before (Corzo et al. 2005). Oxygen and  $H_2S$  microelectrodes were

connected to a picoammeter (PA2000, Unisense®), pH microelectrode to a high impedance mV-meter (MeterLab), and both signals recorded directly to a computer using an A/D converter (ACD-216, Unisense®). Profiles were automated using a motorized micromanipulator connected to a computer and operated by the software Sensor TracePro (Unisense®). In each core, three different vertical profiles of O<sub>2</sub> (detection limit: 0.3–1 μM), pH (resolution 0.1 units) and H<sub>2</sub>S (detection limit: 0.3–1 μM) were measured in random positions on every sampling date. These repeated non-destructive measurements over time in the same cores are possible due to the slim diameter of the microsensors (25 μm at the tip).

Speciation of hydrogen sulfide in solution depends on pH, salinity and temperature (Millero et al. 1988) and since, microsensors can only measure H<sub>2</sub>S, the amount of S<sup>2-</sup> total (S<sub>tot</sub><sup>2-</sup> = H<sub>2</sub>S + HS<sup>-</sup> + S<sup>2-</sup>) was calculated from parallel pH measurements in given experimental conditions. For a pH < 9, S<sub>tot</sub><sup>2-</sup> can be calculated from Eq. (2):

$$[S_{\text{tot}}^{2-}] = [H_2S] (1 + K_1/[H^+]) \quad (2)$$

where K<sub>1</sub> is the first dissociation constant of H<sub>2</sub>S, and [H<sub>2</sub>S] and [H<sup>+</sup>] are the concentrations of H<sub>2</sub>S and protons measured with the H<sub>2</sub>S and pH microsensors, respectively. K<sub>1</sub> can be calculated from pK<sub>1</sub> according to Eq. (3):

$$\text{p}K_1 = -98.08 + 5765.4/T + 15.04555 \\ \times \text{Ln}(T) - 0.127 \times S^{0.5} + 0.0135 \times S \quad (3)$$

where T is temperature (Kelvin), Ln is Napierian Logarithm and S is salinity (Millero et al. 1988). In our experimental conditions with a salinity of 0.33 and a temperature of 13°C, pK<sub>1</sub> of the first dissociation reaction was 7.11. Given this pK<sub>1</sub> and the range of pH measured in the water column and the sediment, H<sub>2</sub>S always accounted for almost 100% of S<sub>tot</sub><sup>2-</sup>. HS<sup>-</sup> was only scarcely relevant in the deepest layer of the sediment where pH was higher than 6.

#### Biogeochemical modelling and acidity net production calculations

Depth profiles of production/consumption and areal integrated rates for O<sub>2</sub>, H<sub>2</sub>S, H<sup>+</sup>, Fe and SO<sub>4</sub><sup>2-</sup> were calculated by biogeochemical modelling based on measured concentration profiles using the PROFILE

software (Berg et al. 1998). Free solution molecular diffusion coefficients for O<sub>2</sub>, H<sub>2</sub>S, H<sup>+</sup>, Fe<sup>2+</sup>, and SO<sub>4</sub><sup>2-</sup> were calculated using the R package MAR-ELAC (Soetaert et al. 2010). To ensure that the calculus domain could be extended to the sediment surface for Fe<sup>2+</sup> and SO<sub>4</sub><sup>2-</sup>, their concentrations at the sediment surface were extrapolated by setting a diffusive boundary layer thickness equal to that obtained from microscale O<sub>2</sub> profiles (i.e. 400–500 μm).

Net production rates of acidity within the sediment can be assumed to nearly equal the fluxes from sediment to water column since the downward directed flux was minimal (about 5% of net production). Net production rates of acidity were estimated by the addition of the contribution of each acidity component according to:

$$R_{\text{acidity}} = \sum_{i=1}^N n_i R_i \quad (4)$$

where R<sub>acidity</sub> is the areal integrated rate of net production or consumption of acidity (meq m<sup>-2</sup> h<sup>-1</sup>), N is the total number of acidity components, n<sub>i</sub> is the number of equivalents per mole of the i<sub>th</sub> species and R<sub>i</sub> is the areal integrated rate of production/consumption of the i<sub>th</sub> species (μmol m<sup>-2</sup> h<sup>-1</sup>). R<sub>i</sub> was previously calculated by numerical modelling the concentration profiles of each component (Berg et al. 1998). Previous studies on acid lakes used Eq. (4), but iron transformation rates were the only source of acidity (Peine et al. 2000). However, according to Eq. (1) more chemical species should be considered to explain acidity fluxes in the Sancho reservoir (i.e. Al, Fe(II), Mn, Zn, Cu, Co, and pH). Thus, Eq. (4) involves a multicomponent budget analogous to those carried out for the estimation of alkalinity fluxes in similar systems (Carignan 1985).

#### Statistical analysis

Data for the different variables are presented as mean ± standard error. A three-way permutational analysis of variance (PERMANOVA) using Euclidean distances was applied to test for differences between C<sub>org</sub>, N, S, and C:N ratio (mol:mol) in the upper 2 cm at the end of every stage (HI, OX and HF) with stage and depth as fixed factors and core identity as a random factor nested within stage. A post hoc pairwise



comparison was performed where a factor was significant at a level of  $p < 0.05$ .

## Results

### Oxygen

Mean  $O_2$  concentration in the mesocosm water column was about 7% of saturation ( $24 \mu\text{mol } O_2 \text{ L}^{-1}$ ) during the initial hypoxic conditions (HI) (Fig. 1a). Oxygen microprofiles at the sediment–water interface indicated that  $O_2$  was consumed within the upper 1 mm sediment layer (Fig. 2a). During the oxic stage (OX) of the experiment,  $O_2$  concentration in the water column rose to about 100% saturation ( $307\text{--}327 \mu\text{mol } O_2 \text{ L}^{-1}$ ). Oxygen penetration depth ( $z_{\text{ox}}$ ) in this period increased with time; from  $\sim 2$  mm the day after oxygenation to  $\sim 6$  mm on day 50 (Fig. 2a). Oxygen profiles and  $z_{\text{ox}}$  similar to the initial ones were measured at the final hypoxic stage (HF).

Biogeochemical modeling of  $O_2$  profiles allowed detecting sediment layers with different net  $O_2$  consumption rate (Fig. 3a–c). In HI, maximum rates of net  $O_2$  consumption occurred in a narrow upper layer slightly below the sediment–water interface, whereas at the end of OX, net  $O_2$  consumption was maximum at the bottom of the oxic layer. The integrated net  $O_2$  consumption rate, which represents the diffusive flux of  $O_2$  to the sediment (Diffusive oxygen uptake, DOU), experienced a steep increase from HI ( $0.21 \pm 0.07 \text{ mmol } O_2 \text{ m}^{-2} \text{ h}^{-1}$ ) to OX ( $2.20 \pm 0.69 \text{ mmol } O_2 \text{ m}^{-2} \text{ h}^{-1}$ ) remaining at similar levels during the first 10 days and decreasing to values 4 times lower at the end of OX. During HF, DOU returned to levels similar to HI (Fig. 4a).

### Sulfide, sulfate, and total sulfur

Hydrogen sulfide was never detected in the water column during the experiment. However, microsensor measurement detected variable amounts of  $H_2S$  within the sediment, up to  $50 \mu\text{mol } L^{-1}$ , under both hypoxic and oxic conditions (Fig. 2b). Vertical profiles of  $H_2S$  were variable, although they presented typically a subsurface peak between 5 and 10 mm below the sediment surface (Fig. 2b), indicating the presence of a narrow production layer at this depth. Although,  $H_2S$

represented almost 100% of total sulphide ( $S_{\text{tot}}^{2-}$ ),  $H_2S$  profiles were transformed to  $S_{\text{tot}}^{2-}$  profiles to calculate production and consumption rates. Produced  $S_{\text{tot}}^{2-}$  was quickly consumed in the upper sediment layer (about 500  $\mu\text{m}$  thick) and more slowly toward deeper sediment layers (Fig. 3d–f).

Net  $S_{\text{tot}}^{2-}$  production rates increased from 50 to  $233 \mu\text{mol } m^{-2} \text{ h}^{-1}$  after 50 days in OX, decreasing immediately in HF to levels similar to those measured in HI (Fig. 4b). Net  $S_{\text{tot}}^{2-}$  oxidation rates above the production layer were  $26.0$  and  $1.5 \mu\text{mol } m^{-2} \text{ h}^{-1}$  in HI and HF respectively, and up to  $139.1 \mu\text{mol } m^{-2} \text{ h}^{-1}$  after 50 days in OX. Usually, the bottom consumption layer tended to be wider than the upper oxic layer and with lower volumetric  $H_2S$  oxidation rates (Figs. 3d–f, 4b). Hydrogen sulfide was found significantly deeper when  $z_{\text{ox}}$  increased ( $r = 0.89$ ,  $\alpha = 0.05$ ) and generally a small overlap existed between the final part of  $O_2$  profiles and the beginning of  $H_2S$  or  $S_{\text{tot}}^{2-}$  profiles (Figs. 2, 3).

Sulfate concentration in the pore water decreased exponentially with depth, reaching levels below detection limit at 5 cm depth. Sulfate increased reversibly from  $0.4$  to  $2.1 \text{ mmol } L^{-1}$  in the pore water of the first cm of sediment and from  $1.2$  to  $1.6 \text{ mmol } L^{-1}$  in the water phase during OX, decreasing both in the sediment and the water column in HF (Figs. 1b, 5a). Biogeochemical modelling of  $SO_4^{2-}$  profiles confirmed the net uptake of  $SO_4^{2-}$  by sediment ( $44 \mu\text{mol } SO_4^{2-} \text{ m}^{-2} \text{ h}^{-1}$ ) in HI, while in OX, due to the strong and reversible increase of net  $SO_4^{2-}$  production, the sediment became a net source of  $SO_4^{2-}$  for the water column ( $70 \mu\text{mol } SO_4^{2-} \text{ m}^{-2} \text{ h}^{-1}$ ) (Fig. 6a). The change to HF reversed the direction of the net flux and almost 95% of the  $SO_4^{2-}$  net consumption within the sediment was supported by  $SO_4^{2-}$  uptake from the water column (Fig. 6a).

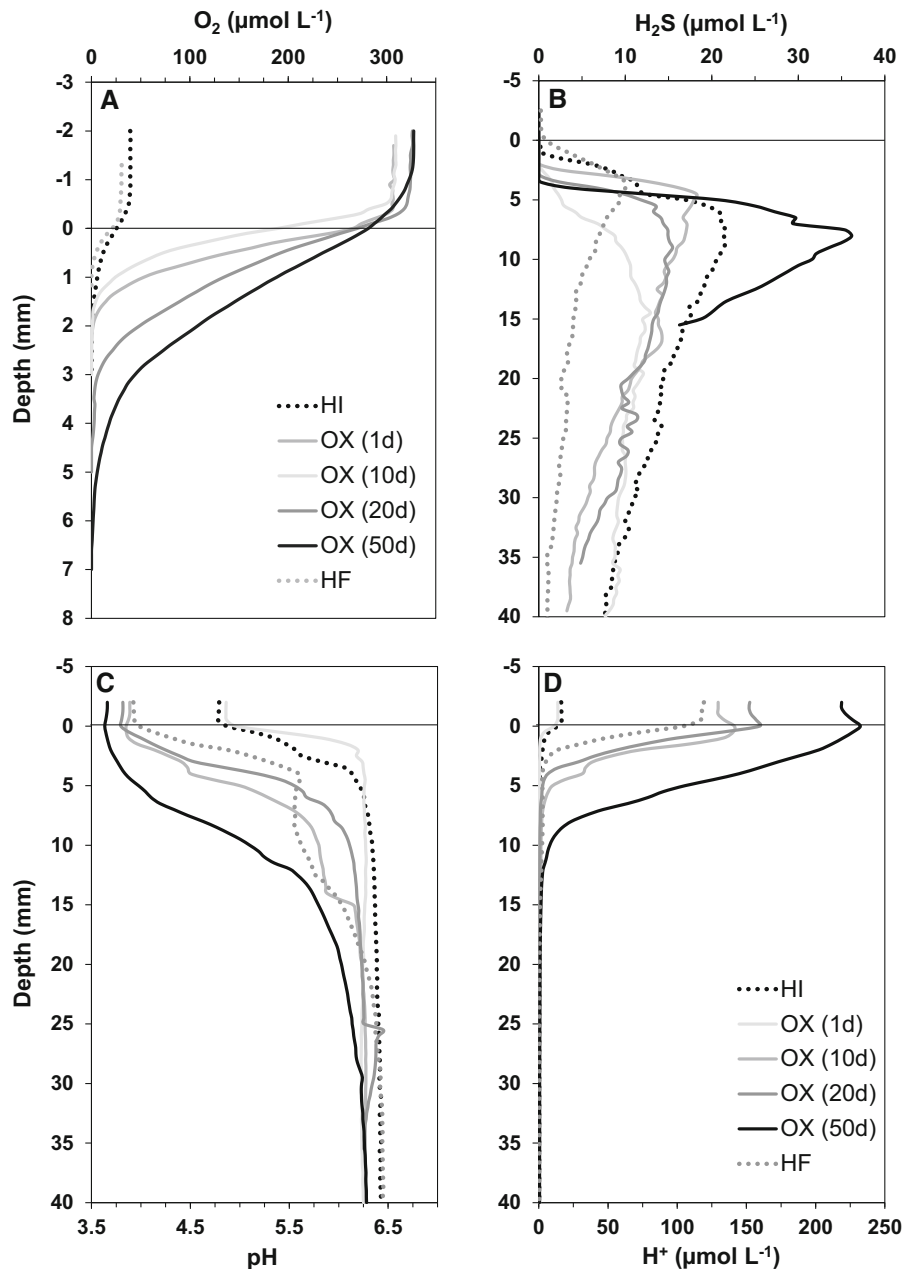
Total S content varied only in upper 2 cm between the three experimental stages, whereas deeper sediment layers remained basically unaffected (result not shown, see Torres et al. 2014). Thus, mean concentrations of S at the end of every stage were calculated for the upper 2 cm layer only (Table 2). Total S decreased significantly ( $2 \text{ mg } cm^{-3}$ ) after 50 days in OX, while no change was observed after 10 days in HF (Table 2).

## pH and proton flux

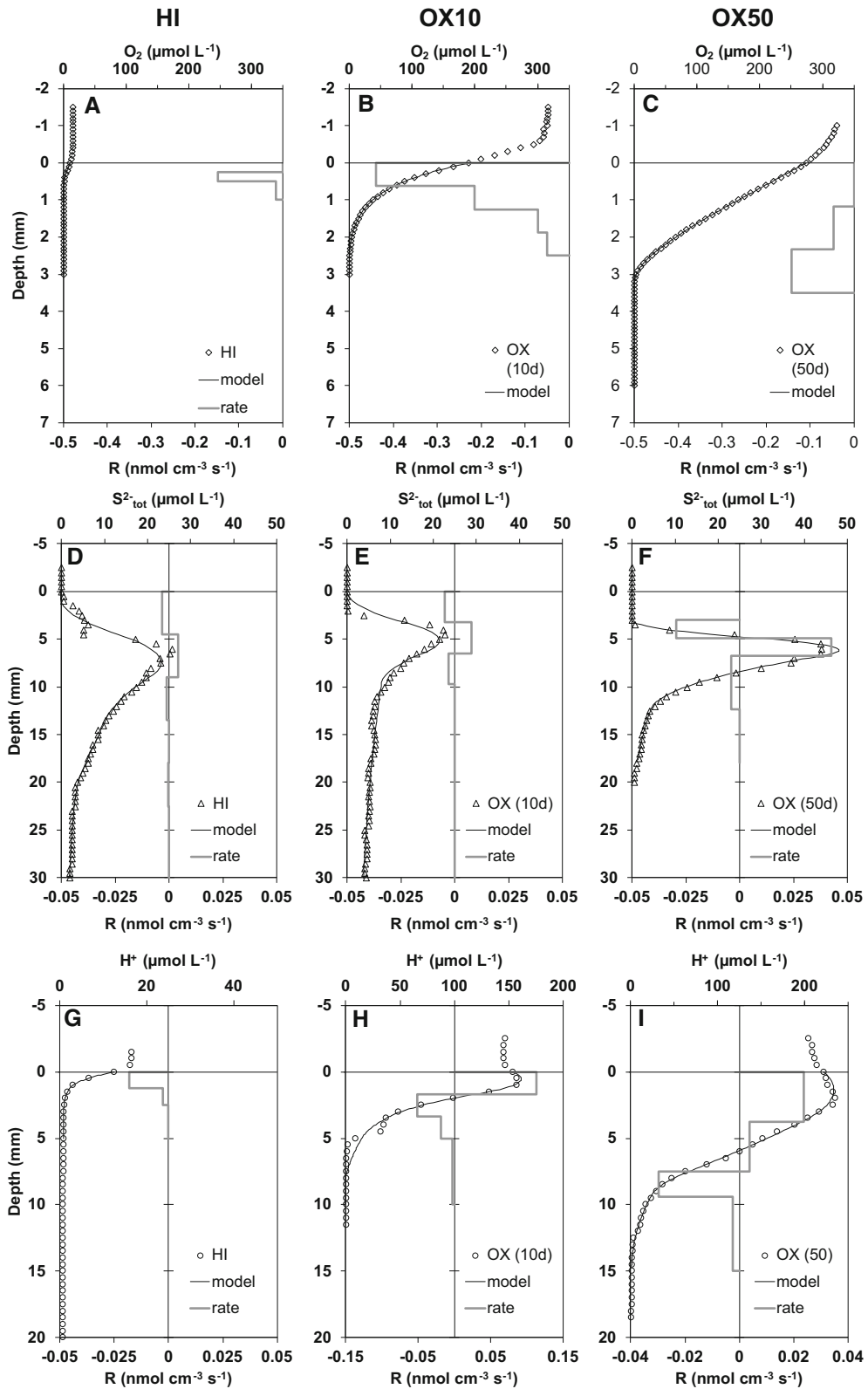
The pH measured in the bulk water phase in HI was 4.6 (Figs. 1, 2), similar to that measured in situ close to the sediment surface when cores were collected (data not shown). The pH in the sediment increased with depth, reaching a maximum pH of 6.5 (Fig. 2c). In OX, the

**Fig. 3** Representative profiles of  $O_2$  (a–c),  $S_{tot}^{2-}$  (d–f) and  $H^+$  (g–i) concentrations in the initial hypoxic conditions (first column), after 10 days in oxic conditions (middle column) and after 50 days in oxic conditions (last column). Dots are experimental data. Black solid lines are the modeled profile (model). Vertical grey lines indicate net production/consumption rates (bottom axis) calculated for different sediment layers by the model

**Fig. 2** Mean  $O_2$  (a),  $H_2S$  (b), pH (c) and  $H^+$  (d) microprofiles at the sediment–water interface at different times during the three experimental stages: initial hypoxic (HI), oxic (OX) and final hypoxic (HF) conditions. Every plotted profile is a mean of 3–9 profiles. Notice the different depth scales in A compared with B, C, and D panels







pH near the sediment–water interface decreased respect to HI and the depth at which the maximum pH was observed increased during OX. Bulk water column pH decreased to 3.7 in the first 10 days in OX.

Proton concentration profiles were calculated from pH profiles to determine the changes in  $H^+$  fluxes at the sediment–water interface during the oxic-hypoxic transitions (Figs. 2d, 3). Consumption of  $H^+$  was restricted to a very narrow upper layer coincident with  $z_{ox}$  in HI (Fig. 3g). After the transition to OX, the  $H^+$  consumption profile changed reversibly to production profile and a clear net  $H^+$  production layer developed in the upper oxic sediment layer. Below the net  $H^+$  production layer, a strong net consumption of  $H^+$  was observed in OX (Fig. 3f). Maximum increase in integrated  $H^+$  production occurred in the first 20 days in OX, but since  $H^+$  consumption increased similarly as well, the net  $H^+$  efflux from the sediment to the water column ( $138.35 \pm 28.03 \mu\text{mol } H^+ \text{ m}^{-2} \text{ h}^{-1}$ ) was important only from day 20 in OX (Fig. 4c).

#### Organic carbon and nitrogen

Dissolved organic carbon (DOC) and dissolved organic nitrogen (DON) increased initially from 300 to  $375 \mu\text{mol DOC L}^{-1}$  and from 39 to  $51 \mu\text{mol DON L}^{-1}$  in OX, decreasing slowly until the end of this stage (Fig. 1f). The transition from OX to HF induced the immediate release of DOC and DON from the sediment as well. Differences in the  $C_{org}$  and N content of the sediment were observed only in the upper 2 cm of the sediment column (Table 2). Mean  $C_{org}$  decreased only  $1 \text{ mg cm}^{-3}$  after 50 days in OX, however, this difference was not statistically significant. However,  $C_{org}$  decreased  $4 \text{ mg cm}^{-3}$  after 10 days in HF, being the decrease in the sediment coincident with an increase in DOC ( $60 \mu\text{mol L}^{-1}$ ) in the water column (Fig. 1f). Sediment N content followed generally the same pattern as  $C_{org}$  during the experiment, whereas the C:N ratio did not change significantly during redox transitions (Table 2).

The dominant form of inorganic N in the water phase was  $\text{NH}_4^+$  (more than 80%) during the entire experiment. Concentrations of  $\text{NH}_4^+$  increased in OX, showing a peak after 6 days that coincided with a peak in DOC (Fig. 1e). Thereafter, concentrations increased steadily up to a maximum of  $175 \mu\text{mol L}^{-1}$  at the end of OX, followed by a sharp decrease after

the change to HF.  $\text{NO}_2^-$  and  $\text{NO}_3^-$  were almost undetectable during OX, but the sediment released small amounts of  $\text{NO}_2^-$  (result not shown) and relatively larger amounts of  $\text{NO}_3^-$  after the change to HF. Phosphate and total dissolved P remained always below detection limits.

#### Iron, aluminium and acidity

Iron concentration in the pore water and water column were similar in HI but changed considerably in OX. Fe content in the water column initially increased slightly but became undetectable after 10 days in OX (Fig. 1b), while Fe increased in the pore water, from 0.13 to  $0.77 \text{ mmol Fe L}^{-1}$  at the sediment surface after 50 days in OX (Fig. 5b). Both Fe production rate in the pore water ( $245 \mu\text{mol Fe m}^{-2} \text{ h}^{-1}$ ) and net flux towards the water column increased in OX compared to HI (Fig. 6b). The Fe released to the oxic water column immediately precipitated as schwertmannite in OX (result not shown, see Torres et al. 2014). Fe content in the pore water decreased immediately in HF due to the decrease in Fe net production (50%), whereas at the same time a strong increase of Fe in the water column was observed, despite of a lower efflux rate, most likely because the released Fe remained in solution in the hypoxic water column.

Aluminium concentration in the water column was also notably affected by  $\text{O}_2$ , increasing in OX and decreasing in HF (Fig. 1d). Acidity in the water column followed a trend similar to Al, after an initial transient decrease, increased strongly ( $0.75 \text{ meq m}^{-2} \text{ h}^{-1}$ ) up to  $1.05 \text{ meq L}^{-1}$  at day 30 and remained constant the last 20 days of OX (Fig. 1d). Acidity within the sediment was similar to that of water column and increased considerably in the upper 5 cm layer in OX ( $1.64 \text{ meq L}^{-1}$ ), being higher than the water column (Fig. 5c). The reestablishment of hypoxic conditions did not change significantly the acidity in the water column, while Al decreased clearly. On the contrary, acidity in the sediment reversed back to initial conditions with the exception of the surface layer.

The contribution of Al, Fe,  $H^+$  and other elements to acidity in the water column and sediment changed in different ways during redox transitions. In the water column, Al, Fe and  $H^+$  contributions to acidity, estimated from Eq. (1), were 44, 36 and 1.5% respectively in HI. However, since Fe disappeared

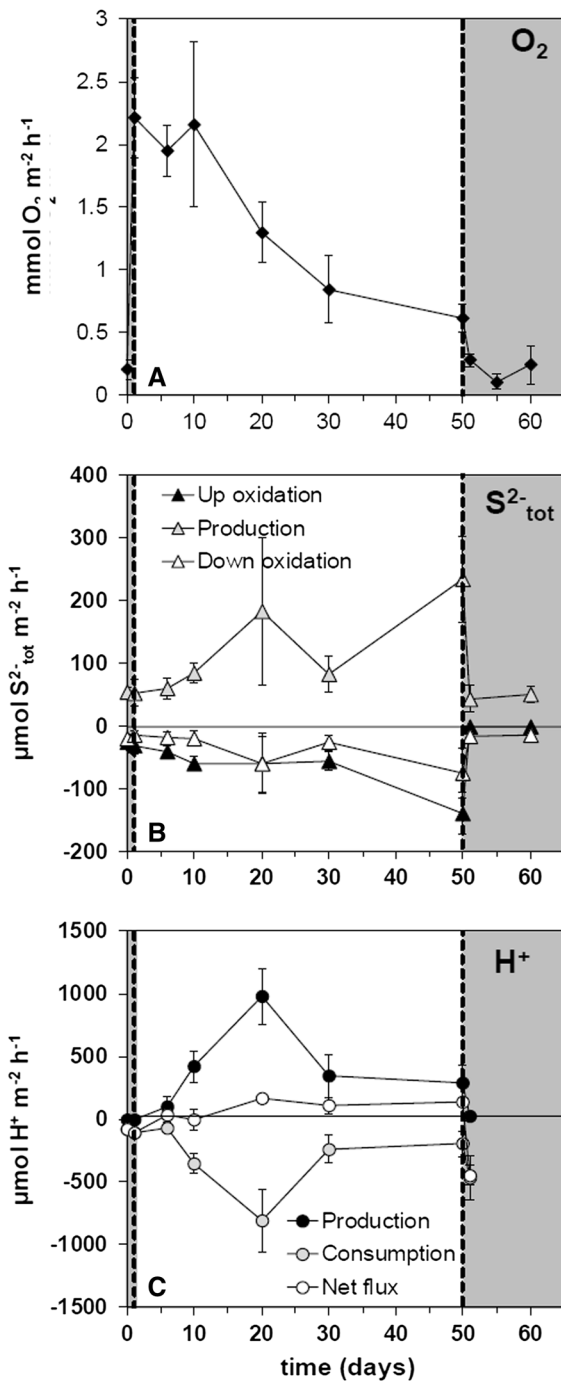


**Fig. 4** Temporal evolution of diffusive O<sub>2</sub> uptake rate (a), net rates of S<sub>tot</sub><sup>2-</sup> production and oxidation within the sediment (b), and net H<sup>+</sup> production and consumption within the sediment and net H<sup>+</sup> flux across the sediment–water interface (b). Values were estimated from modelled profiles as shown in Fig. 3. Negative and positive values indicate net consumption and net production, respectively. Data are means ± standard errors of 6 different profiles (2 profiles × 3 cores). Areas shaded in grey indicated initial and final hypoxic conditions periods

to water column, Fe was always the main contributor (65–98%) to pore water acidity, with the contributions of Al and pH being minimal under hypoxic and oxic conditions. The flux of acidity indicated a net sediment consumption (0.08 meq m<sup>-2</sup> h<sup>-1</sup>) in HI that changed to production of acidity within the upper sediment layers in OX, being partially exported to the water column (0.52 meq m<sup>-2</sup> h<sup>-1</sup>) after 50 days in OX. These changes reversed in HF (Fig. 6c).

**Discussion**

Oxygen uptake at the sediment–water interface

Benthic oxygen flux has been shown to depend on several factors including organic carbon content, upward flux of reduced inorganic species, O<sub>2</sub> concentration, temperature, water turbulence and bioirrigation (Rabouille and Gaillard 1991; Cai and Reimers 1995; Lorke et al. 2003; Glud 2008). In our experimental conditions, temperature and water turbulence can be considered constant whereas bioirrigation does not exist since sediment cores were collected in anoxic conditions. Therefore, only diffusive fluxes will be considered.

Diffusive oxygen uptake (DOU) rates at the sediment water interface were in the range or slightly higher than those available in the literature for acid lakes (Kühl et al. 1998; Koschorreck et al. 2003; Lagauzère et al. 2011) and neutral lakes (Sweerts et al. 1991; Maerki et al. 2009; Matzinger et al. 2010; Schwefel et al. 2017). The instantaneous increase in O<sub>2</sub> concentration in the HI-OX transition probably induced an increase in the oxidation rates of organic matter and reduced compounds like Fe<sup>2+</sup>, S<sub>tot</sub><sup>2-</sup> (mainly as H<sub>2</sub>S), and metallic sulfides, among others (Table 1). However, DOU decreased during OX likely due to a concurrent decrease of labile organic matter and reduced inorganic compounds. In addition, the relative

from the water column in OX, the increase in acidity in this stage was mainly a consequence of the increase in Al, increasing its contribution to acidity as well (68.9%), the rest being attributed to increases in H<sup>+</sup> (about 6%) and Zn, Co, Ni, and Cu in the water column (results not shown, see Torres et al. 2014). In contrast

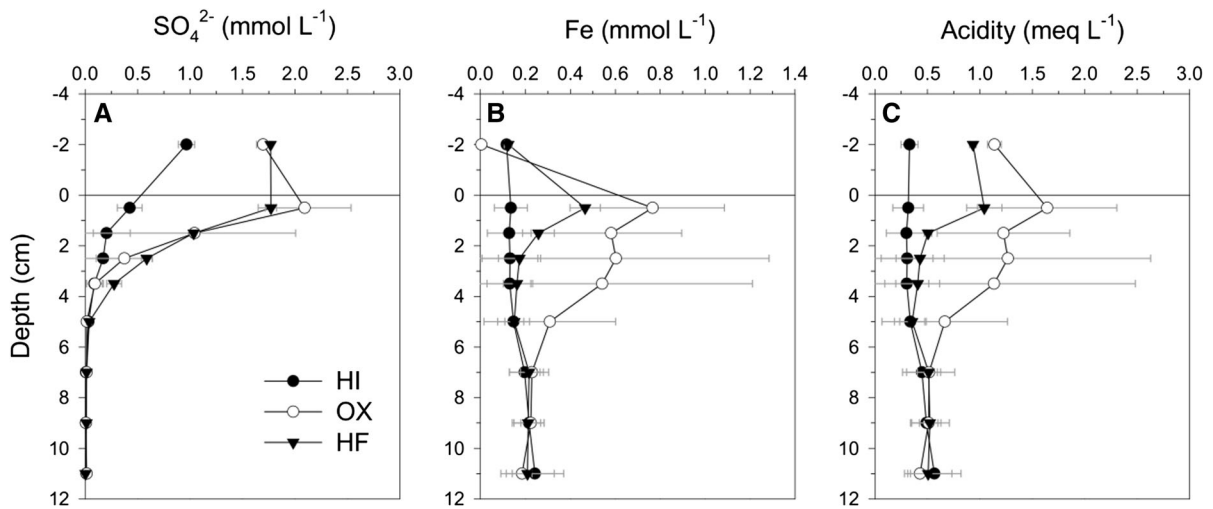


**Fig. 5** Vertical pore water profiles of sulfate, Fe and acidity at the end of each experimental stages: initial hypoxic (HI), oxic (OX) and final hypoxic (HF) conditions. Every plotted profile is a mean  $\pm$  SE of 3 cores

contribution of these compounds to DOU likely changed during the experiment.

The changes in the partition of the DOU between different process (organic matter mineralization, sulfide and  $\text{Fe}^{2+}$  oxidation) during the redox transitions was estimated through several complementary approaches (Supplementary Tables S1, S2). The fraction of DOU due to the oxidation of  $\text{S}_{\text{tot}}^{2-}$  ( $\text{DOU}_{\text{S}}$ ) can be estimated from the  $\text{S}_{\text{tot}}^{2-}$  oxidation rates calculated from the modeling of  $\text{S}_{\text{tot}}^{2-}$  profiles in the oxic layer (up oxidation, Fig. 4) and the stoichiometry of reaction 6 (Table 1).  $\text{DOU}_{\text{S}}$  consumed  $0.054 \text{ mmol O}_2 \text{ m}^{-2} \text{ h}^{-1}$  in HI, increasing to  $0.281 \text{ mmol O}_2 \text{ m}^{-2} \text{ h}^{-1}$  after 50 days in OX. These calculations indicate that in HI about 26% of DOU was due to the oxidation of  $\text{S}_{\text{tot}}^{2-}$ , while in OX the contribution of  $\text{DOU}_{\text{S}}$  to DOU changed from a minimal contribution during the first 10 days (4%) to 46% after 50 days (Table S2). Similar seasonal variability in  $\text{H}_2\text{S}$  oxidation rates has been found in field studies (Sweerts et al. 1991; Urban et al. 1994). Our calculations assume that  $\text{S}_{\text{tot}}^{2-}$  is oxidized in the upper oxidation layer only by  $\text{O}_2$ . However,  $\text{S}_{\text{tot}}^{2-}$  can be oxidized by  $\text{FeOOH}_{(\text{s})}$  as well, so the estimation of  $\text{O}_2$  consumption by  $\text{S}_{\text{tot}}^{2-}$  oxidation represents maximal values. In addition, oxidation of  $\text{S}_{\text{tot}}^{2-}$  to  $\text{S}^{\circ}$  might decouple the temporal changes of  $\text{S}_{\text{tot}}^{2-}$  and  $\text{O}_2$ . However, this process was unlikely in the Sancho sediments because we detected a clear decrease of total S during OX (Table 2).

The fraction of DOU consumed in the mineralization of OM ( $\text{DOU}_{\text{Corg}}$ ) was calculated in several ways. Three out of the four approaches used here (Supplementary Table S1) to calculate  $\text{DOU}_{\text{Corg}}$ , i.e. a mechanistic model based on the Monod equation (Supplementary material, Eq. (1); Rabouille and Gailard 1991; Canavan et al. 2006), an empirical equation (Cai and Reimers 1995) and the difference in  $\text{C}_{\text{Org}}$  during OX, gave very similar estimates.  $\text{DOU}_{\text{Corg}}$  was  $0.08\text{--}0.12$  and  $\text{mmol O}_2 \text{ m}^{-2} \text{ h}^{-1}$  in HI and increased to  $0.40\text{--}0.63 \text{ mmol O}_2 \text{ m}^{-2} \text{ h}^{-1}$  in OX (Supplementary Table S1). In the contrast, the calculation of the OM mineralization based on the  $\text{NH}_4^+$  release rate to the water column during OX produced  $\text{DOU}_{\text{Corg}}$  values 2–3 times higher than those calculated with the other approaches. This approach likely overestimated  $\text{DOU}_{\text{Corg}}$  since part of the  $\text{NH}_4^+$  released to the water column might originate from the exchangeable  $\text{NH}_4^+$  fraction, which is known to be large in lake sediments and is released in OX (Mackin and Aller 1984; Morse and Morin, 2005). In summary, the estimated  $\text{DOU}_{\text{Corg}}$  in HI was about 49% of the total DOU measured with  $\text{O}_2$  microsensors. Of the remaining DOU, 26% was attributed to  $\text{S}_{\text{tot}}^{2-}$  oxidation and the rest 25% to the oxidation of free  $\text{Fe}^{2+}$  and metallic sulfides (Table S2).

Consumption of  $\text{O}_2$  by the oxidation of Fe and other metallic sulfides ( $\text{DOU}_{\text{MS}}$ ) can be estimated as:  $\text{DOU}_{\text{MS}} = \text{DOU} - (\text{DOU}_{\text{S}} + \text{DOU}_{\text{Corg}})$ . The transition to OX increased  $\text{DOU}_{\text{Corg}}$  in absolute terms, but

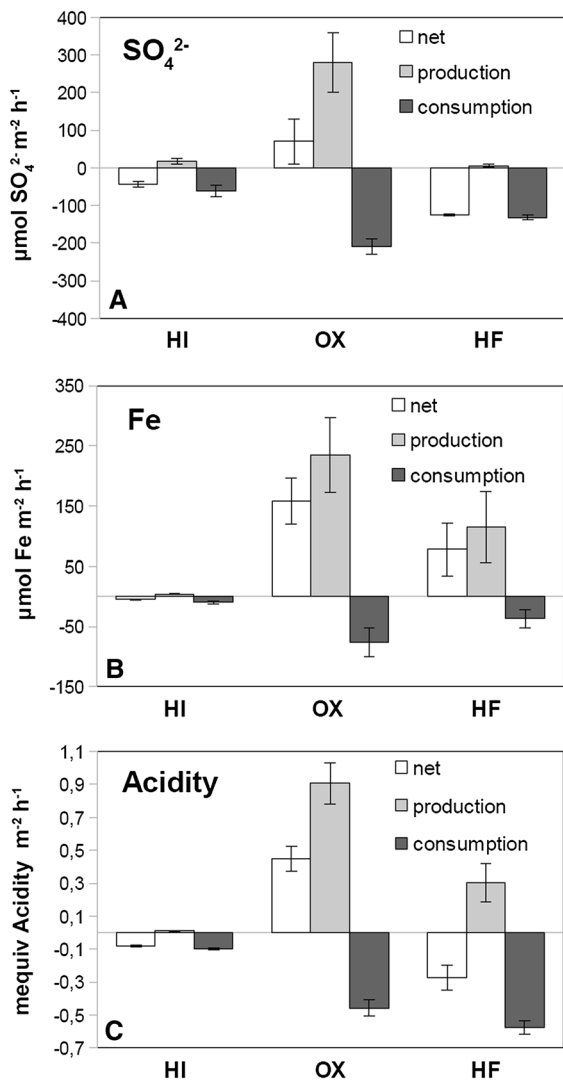


**Fig. 6** Depth integrated  $\text{SO}_4^{2-}$  (a), Fe (b), and acidity (c) production, consumption and net rates in the sediment at the end of each experimental stage: initial hypoxic conditions (HI), 50 days of oxic conditions (OX) and 10 days of hypoxic conditions (HF). Values were estimated from modelled profiles as shown in Fig. 3

this rate was only 20–26% of the measured transient increase in total DOU during the first 10 days in OX. These calculations indicated that the  $\text{DOU}_{\text{MS}}$  represented 68–79% of total  $\text{O}_2$  uptake during the first 10 days of OX. However, after 50 days in OX no oxygen consumption could be attributed to metallic sulfides oxidation; the sum of aerobic oxidation of organic matter plus  $\text{S}_{\text{tot}}^{2-}$  oxidation was similar to the total  $\text{O}_2$  consumption rate measured by  $\text{O}_2$

**Table 2** Total sulfur (S), organic carbon ( $\text{C}_{\text{org}}$ ), and total nitrogen (N) content ( $\text{mg cm}^{-5}$ ), and  $\text{C}_{\text{org}}:\text{N}$  ratio (mol:mol) in the upper 2-cm layer of sediment, in the initial hypoxic stage of the experiment (HI), after 50 days in oxic conditions (OX) and after 10 days in hypoxic conditions (HF)

	S	$\text{C}_{\text{org}}$	N	C:N
HI	$5.7 \pm 0.3^{\text{a}}$	$14.4 \pm 0.7^{\text{a}}$	$1.7 \pm 0.1^{\text{a}}$	$10.9 \pm 0.3^{\text{a}}$
OX	$3.6 \pm 0.6^{\text{b}}$	$13.2 \pm 1.2^{\text{a}}$	$1.5 \pm 0.2^{\text{a}}$	$11.1 \pm 0.5^{\text{a}}$
HF	$3.5 \pm 0.4^{\text{b}}$	$9.2 \pm 1.0^{\text{b}}$	$1.0 \pm 0.1^{\text{b}}$	$11.0 \pm 0.9^{\text{a}}$

Data are presented as mean  $\pm$  standard error ( $n = 3$ ). Superscript letters indicate homogeneous groups tested by pairwise comparison within factor Stage ( $p = 0.05$ )

microsensors. Therefore, these estimates suggest that oxidation of FeS,  $\text{FeS}_2$  and other metal sulfides by  $\text{O}_2$  (Table 1, R10) was very important at the beginning of OX. Its importance decreases or even disappears completely after a prolonged oxic period, once these compounds are exhausted in the oxic layer. The biogeochemical analysis of spatiotemporal changes presented here represent an important improvement of aerobic mineralization of organic matter contribution estimates with respect to previous ones (Torres et al. 2014) and emphasize the importance of C and N cycling at the sediment–water interface in AMD contaminated reservoirs.

#### Sulfur cycling at the sediment–water interface

Net  $\text{S}_{\text{tot}}^{2-}$  production occurred mainly in a narrow layer (200–500  $\mu\text{m}$ ) located immediately below  $z_{\text{ox}}$  in both oxic and hypoxic conditions (Figs. 2b, 3d–f). Sulfide concentrations within the sediments were similar or lower than those measured in other acidic ecosystems of different types (Kühl et al. 1998; Koschorreck et al. 2003; 2007a; Wendt-Potthoff et al. 2012). Net  $\text{SO}_4^{2-}$  reduction rates, calculated either by modelling the pore water profiles of  $\text{SO}_4^{2-}$  or  $\text{S}_{\text{tot}}^{2-}$  were similar, about 60 and 220  $\mu\text{mol SO}_4^{2-} \text{ m}^{-2} \text{ h}^{-1}$  in HI and OX, respectively (Fig. 6a). These net  $\text{SO}_4^{2-}$  reduction rates in the sediment of the Sancho reservoir were in the lower part of the wide range of values available for acid lakes (Holmer and Storkholm 2001; Koschorreck 2008; Wendt-Potthoff et al. 2012).

Counterintuitively, net  $\text{SO}_4^{2-}$  reduction rates were higher during OX than HI or HF (Figs. 4b, 5), due to higher  $\text{SO}_4^{2-}$  availability as consequence of an

increase of oxidation of S-reduced compounds, such as  $S_{\text{tot}}^{2-}$ ,  $Fe_xS$ , other metal sulfides, and possibly organic S, in the presence of higher  $O_2$  concentration and a deeper  $z_{\text{ox}}$  (Kling et al. 1991). In addition to an increase of sulfate reduction, the higher net production of  $SO_4^{2-}$  in the sediment resulted in a net transfer of S to the water column in the form of regenerated  $SO_4^{2-}$  (Table 2, Fig. 1b) (Kling et al. 1991; Holmer and Storkholm 2001; Küsel 2003). Part of this  $SO_4^{2-}$  flux to the water column (about 30%) might be due to the dissolution of hydrobasaluminite as well (Table 1, R13; Sánchez-España et al. 2011). However, once released to the water column, only about 28% of the  $SO_4^{2-}$  remained in the water column during OX according to calculations based on total S and  $SO_4^{2-}$  budgets in the sediment and the water column, respectively. The rest precipitated most likely mainly as schwertmannite (Table 2; R 11), a phenomenon that was most intensely observed in the first 10 days in OX; when schwertmannite covered all solid surfaces within the mesocosm (e.g. tank walls, tank bottom, cores) (Torres et al. 2014).

Net  $SO_4^{2-}$  production rates calculated from the  $S_{\text{tot}}^{2-}$  oxidation or consumption rates in the oxic and the anoxic part of the sediment increased along OX (Fig. 4b). Oxic  $S_{\text{tot}}^{2-}$  oxidation (R6, Table 1) occurred in a narrow layer above the  $SO_4^{2-}$  reduction zone (up oxidation) where  $O_2$  and  $H_2S$  profiles generally overlapped as previously found in other systems (Jørgensen and Revsbech 1983). Turnover times in the  $SO_4^{2-}$  reducing layer and the oxic and anoxic  $S_{\text{tot}}^{2-}$  oxidation layers, assuming constant average concentrations and rates, were about 10, 17, and 86 days, respectively. These values are higher than those reported for biofilms and microbial mats (seconds to hours, Kühl et al. 1992; Dillon et al. 2007), but lower than those for acid lakes (80 days, Koschorreck et al. 2003) or the Black Sea anoxic sediments (about 5 years, Jørgensen et al. 2001).

In the absence of  $O_2$ ,  $S_{\text{tot}}^{2-}$  can (1) be oxidized anaerobically by manganese and iron oxides, either abiotically or biotically by bacteria (Jørgensen and Bak 1991; Jost et al. 2010) (2) precipitate with  $Fe^{2+}$  and other divalent metals to form different metal sulfides (R9 and R10) or (3) be adsorbed to organic matter (Table 1; R11). In the sediment of the Sancho Reservoir, anaerobic consumption of  $S_{\text{tot}}^{2-}$  occurs mainly by oxidation with  $FeOOH$  (Table 1; R7), as

Mn concentration in the pore water and solid phase were very low (Torres et al. 2014). Precipitation of Fe and other metal sulfides during OX in the anoxic sediment layer was most likely of little importance since we observed a decrease in total S within the sediment. In addition to oxic  $S_{\text{tot}}^{2-}$  oxidation, anaerobic  $S_{\text{tot}}^{2-}$  oxidation by R8 probably increased as a consequence of the higher  $FeOOH_{(s)}$  availability in OX due to the oxidation of  $Fe^{2+}$  by  $O_2$  in the water column and sediment (Table 1; R6). Our results clearly show that seasonal redox fluctuations driven by higher availability of  $O_2$  affect the permanent burial of S and metals in the sediment (Küsel 2003; Blodau 2006; Wendt-Potthoff et al. 2012), likely reducing the efficiency of natural attenuation or bioremediation treatments.

#### Protons, iron cycling and acidity exchange at the sediment–water interface

The pH profiles at the sediment–water interface in the Sancho Reservoir were similar to those found in other acid lakes (Koschorreck et al. 2007a, b; Geller et al. 2009). Sediment pH was always higher than in the water column, being the maximum pH gradient, this is the maximum net  $H^+$  consumption layer, at or below the  $z_{\text{ox}}$  (Figs. 2a, c, 3g, h). In the pH range measured in the Sancho sediment,  $H^+$  consumption rates by iron reduction coupled to either organic matter or  $H_2S$  oxidation (Table 1; R4 and R7, respectively) were the main consuming processes, probably an order of magnitude higher than sulfate reduction and denitrification (Table 1; R2 and R3) (Jourabchi et al. 2005; Soetaert et al. 2007). The switch to OX changed the  $H^+$  consumption profile to a production profile, where  $H^+$  production occurred at sediment surface and extended downward during OX (Figs. 2d, 3g–i). This was apparently due to the increase of  $z_{\text{ox}}$  and consequently of aerobic oxidation of  $H_2S$  and  $Fe^{2+}$  followed by the precipitation of Fe(III) oxyhydroxides (Table 1; R5, R6 and R12).

Part of the  $H^+$  produced within the sediment during OX was exported to the water column, changing the role of the sediment from net sink during HI to net source, thus contributing to the observed acidification of the water column (Fig. 1). Two clear successive phases were observed in OX. During the first phase, the increase of  $H^+$  in the water column was 5.5 times



higher than the release from the sediment up to day 10 (Table 3). The main contributor to this increase was probably the precipitation of schwertmannite (Table 1; R12) (Torres et al. 2014). During the second phase (days 20–50), the release of  $H^+$  from the sediment was neutralized (Table 3), likely due to the dissolution of Al hydroxides and hydroxysulfates (Table 1; R13) at the sediment surface (Totsche et al. 2003; Sánchez-España et al. 2011).

The efflux of acidity during OX was in the range of those measured in other acid lakes (Peine et al. 2000) and likely occurred via an efflux of  $Fe^{2+}$  from the sediment to the water column. Reduced iron in water column was immediately oxidized by  $O_2$  over the sediment surface (Table 1; R6), where  $Fe^{3+}$  precipitated mainly as schwertmannite releasing  $H^+$  (Table 1; R12) (Peine et al. 2000; Küsel 2003; Meier et al. 2004). The drop in pH increased the solubility of Al hydroxides, with Al being released to the water column. This, on the one hand, contributed to an increase of acidity and, on the other, to buffer further decreases of pH (Totsche et al. 2003; Sánchez-España et al. 2011). Another very important consequence of the interaction between Fe and Al cycling at the sediment surface is the transfer of  $e^-$  acceptors in the form of Fe(III) minerals from the oxic water column to the sediment, where Fe(III) minerals can support high rates of anoxic oxidation of reduced sulfide minerals and organic matter (Peine et al. 2000; Wendt-Potthoff and Koschorreck 2002; Meier et al. 2004). This mechanism is a drawback for bioremediation of acid pit lakes based on carbon-driven alkalinity generation treatments (Geller et al. 2009; Nixdorf et al. 2010) and should be taken into account in all types of bioremediation strategies in acid mine drainage impacted systems. The dynamics of  $H^+$ , acidity, and the solid and soluble phases of Fe and Al compounds at the sediment–water interface were therefore strongly interconnected and were highly dependent on  $O_2$  availability.

#### Carbon and nitrogen cycling during redox transitions in acidic environments

Despite the special characteristics of the AMD impacted Sancho Reservoir, the  $C_{org}$  and N contents and C:N ratio in the upper sediment layer were within the wide range observed in lakes (Kemp et al. 1977; Meyers and Ishiwatari 1993). Temporal changes in the

$C_{org}$  and N content of the sediment during the redox transition were only restricted to upper 2 cm. In this reactive layer, given an average net sedimentation rate of  $1.6 \text{ cm year}^{-1}$  for this system (Cánovas et al. 2016), OM presumably deposited during the last 1.25 years at most. Redox transitions exerted a strong effect on the exchange of DOC and DON across the sediment–water interface. During HI-OX transition, we observed a transient efflux of DOC and DON from the sediment ( $0.88 \text{ mM DOC m}^{-2} \text{ h}^{-1}$  and  $0.08 \text{ mM DON m}^{-2} \text{ h}^{-1}$ ). Most likely, the higher  $O_2$  availability stimulated aerobic microbial OM degradation within the sediment (Freeman et al. 2001; Arndt et al. 2013), and soluble compounds diffused to the water column. The high efflux of  $NH_4^+$  to the water column during OX (see below) supports an increase of OM degradation. In addition, the pH and redox changes in OX could have affected the adsorption–desorption balance of OM to sediment particles releasing OM adsorbed during the previous anoxic conditions (Sinninghe Damste and De Leeuw 1990; Zonneveld et al. 2010). The decrease of DOC and DON during the second half of OX was probably due to (1) their co-precipitation with mineral phases of Fe(III), mostly Fe(III) oxyhydroxysulfates like schwertmannite or jarosite (Küsel 2003; Meier et al. 2004), and (2) to the formation of macromolecular iron-organic carbon complexes, which has been shown to increase the transfer of OM to the sediment and protects it from degradation (Eglinton 2012; Lalonde et al. 2012; Barber et al. 2017). The overall result was the partial return of the DOC and DON released to the water column back to the sediment, which explains the minimal difference observed in  $C_{org}$  between HI and OX (Table 2).

Interestingly, we observed larger and statistically significant differences in  $C_{org}$  and N sediment contents after 10 days in HF. The decrease of  $5.3 \text{ mg } C_{org} \text{ cm}^{-3}$  in HF was likely due to its release again to the water phase as DOC ( $0.42 \text{ mM DOC m}^{-2} \text{ h}^{-1}$ ) due to re-dissolution of ferric hydroxides and a subsequent desorption of bound organic compounds (Gu et al. 1995; Skoog et al. 2009; Riedel et al. 2013). The DOC:Fe stoichiometric ratio of the released DOC and Fe after dissolution of Fe hydroxides– $C_{org}$  complex was about 0.46 probably due to the relatively long exposure to oxygen during the OX (Lalonde et al. 2012; Barber et al. 2017). Similarly, nitrogen in the sediment decreased significantly, suggesting the release of DON to the water phase ( $0.11 \text{ mM}$

DON  $\text{m}^{-2} \text{h}^{-1}$ ) also due to the dissolution of ferric hydroxides.

Both DOC and DON were released right after each redox transition; however, the DOC:DON ratio was very different in each case. The DOC:DON ratio (10.8) was similar to that of sediment OM at the beginning of OX, but this ratio was considerably lower (3.7) after the transition to HF, suggesting that dissolved OM released in HF was considerably enriched in N. This observation deserves further study and it might be due to a higher co-precipitation of DON and  $\text{NH}_4^+$  with Fe(III) hydroxides compared to DOC during OX.

Inorganic nitrogen was relatively high in our system. Probably, P low concentration due to sorption to ferric hydroxides as in other acid lakes (Beulker et al. 2003; Moser and Weisse 2011) lead to a low N demand overall. The most abundant species of inorganic nitrogen in our experiment was  $\text{NH}_4^+$ , probably due to the inhibition of nitrification in acid lakes (Jeschke et al. 2013). The transition to oxic conditions almost doubled sediment ammonification rates within the first 6 days, resulting in the release of  $\text{NH}_4^+$  to the water column ( $0.5 \text{ mmol NH}_4^+ \text{ m}^{-2} \text{ h}^{-1}$ ). This increase in  $\text{NH}_4^+$  coincided with that of DOC. However, contrary to DOC and DON,  $\text{NH}_4^+$  kept increasing during OX ( $0.1 \text{ mmol NH}_4^+ \text{ m}^{-2} \text{ h}^{-1}$ ). This  $\text{NH}_4^+$  release rate is in the range of those found in neutral fresh water environments, including eutrophic and hypereutrophic lakes (Burger et al. 2007; Kuwabara et al. 2009). In our experimental conditions, the release of  $\text{NH}_4^+$  in OX might be due to an increase in the mineralization of  $\text{C}_{\text{org}}$  (Supplementary material, Table S1) and its release from the exchangeable  $\text{NH}_4^+$  fraction of the sediment (Mackin and Aller 1984; Morse and Morin 2005).

The sudden decrease in  $\text{NH}_4^+$  and the parallel release of  $\text{NO}_2^-$  (result not shown) and  $\text{NO}_3^-$  from the

sediment in HF was a rather unexpected result (Fig. 1d). Recently, the anaerobic oxidation of  $\text{NH}_4^+$  to  $\text{N}_2$ ,  $\text{NO}_2^-$  or  $\text{NO}_3^-$  coupled to Fe(III) reduction (Feammox), has been suggested in different iron reducing environments (Clément et al. 2005; Yang et al. 2012; Huang and Jaffé 2015). This process is thermodynamically favorable at the low pH ( $\leq 4$ , Thamdrup 2012) found in AMD contaminated systems, and could be the responsible for the production and release of  $\text{NO}_2^-$  and  $\text{NO}_3^-$  from the sediment in HF. Since nitrification is inhibited in acid lakes, Feammox might play a very important role in cycling of inorganic N in acids lakes. Further research, beyond the scope of this work, is needed to demonstrate the role of Feammox in the cycling of N and Fe in acidic environments such as the Sancho Reservoir.

## Conclusions

The results presented here highlight the close and complex coupling between the C, N,  $\text{O}_2$ ,  $\text{H}^+$ , S, Fe and Al cycles across the sediment–water interface during redox transitions in acid aquatic environments. In oxic conditions, the release of  $\text{H}^+$ ,  $\text{SO}_4^{2-}$ ,  $\text{Fe}^{2+}$  and  $\text{Al}^{3+}$  to the water column represents a combined mechanism of acidity and electrons transfer from the sediment to the oxic water column mediated by (1) the efflux of  $\text{H}^+$  and dissolved Fe(II), with additional smaller contributions of other metals, (2) the reoxidation of Fe(II) to Fe(III) and the high stoichiometric  $\text{H}^+$  production associated with the precipitation of schwertmannite, and (3) the  $\text{H}^+$  consumption during the dissolution of Al-hydroxides and hydroxysulfates at the sediment surface, with Al being the main contributor to water column acidity in OX. The precipitation of Fe(III) and  $\text{SO}_4^{2-}$  as schwertmannite also represents a mechanism of reintroduction of regenerated  $\text{e}^-$  acceptors to the

**Table 3** Net  $\text{H}^+$  flux rate at sediment–water interface averaged over the duration of each period, expected net increase of  $\text{H}^+$  in the water column based on the  $\text{H}^+$  net fluxes and

measured net  $\text{H}^+$  increase (Measured  $\Delta \text{H}^+$ ) in the water column determined from the difference in pH values at the beginning and the end of each period

	Net $\text{H}^+$ flux rate ( $\mu\text{mol m}^{-2} \text{ h}^{-1}$ )	Expected $\Delta \text{H}^+$ ( $\mu\text{mol L}^{-1}$ )	Measured $\Delta \text{H}^+$ ( $\mu\text{mol L}^{-1}$ )
OX: 1–10 days	50.68	11.56	63.21
OX: 20–50 days	123.17	112.41	– 1.80
HF: 50–51 days	– 444.22	– 10.13	– 3.5

sediment, which allows further anaerobic oxidation of organic and inorganic reduced compounds. Redox transitions affect the exchange of dissolved C and N between the water column and the sediment by (1) controlling the degradation rate of OM, which depends strongly on the availability electron acceptors, and (2) affecting the physicochemical adsorption–desorption of different organic compounds to sediment particles and their co-precipitation with Fe(III) hydroxides due to redox and pH changes. The unexpected release of  $\text{NO}_2^-$  and  $\text{NO}_3^-$  in the oxic–hypoxic transition, in parallel with the decrease in  $\text{NH}_4^+$  in the water column, might indicate the presence of Feammox in the sediment of acid lakes for the first time and it might represent an alternative way to nitrification to regenerate  $\text{NO}_3^-$ . The prediction of the rates and final outcome of natural attenuation processes and bioremediation treatments requires a better understanding of the multiple biogeochemical effects of redox transitions at the sediment–water interface.

**Acknowledgements** The research was funded by projects P11-RNM-7199 from the Junta de Andalucía and CTM2013-43857-R, CTM2017-82274-R, CGL2013-48460-CO2, CTM2014-61221-JIN and CGL2016-78783-C2-2-R from the Spanish I + D + I Program. J. L. Jiménez Arias was funded by a PhD grant (Ref:2010-063) from the University of Cadiz.

**Open Access** This article is distributed under the terms of the Creative Commons Attribution 4.0 International License (<http://creativecommons.org/licenses/by/4.0/>), which permits unrestricted use, distribution, and reproduction in any medium, provided you give appropriate credit to the original author(s) and the source, provide a link to the Creative Commons license, and indicate if changes were made.

## References

- Arndt S, Jørgensen BB, LaRowe DE et al (2013) Quantifying the degradation of organic matter in marine sediments: a review and synthesis. *Earth Sci Rev* 123:53–86. <https://doi.org/10.1016/j.earscirev.2013.02.008>
- Barber A, Brandes J, Leri A et al (2017) Preservation of organic matter in marine sediments by inner-sphere interactions with reactive iron. *Sci Rep* 7:366. <https://doi.org/10.1038/s41598-017-00494-0>
- Belias C, Dassenakis M, Scoullou M (2007) Study of the N, P and Si fluxes between fish farm sediment and seawater. Results of simulation experiments employing a benthic chamber under various redox conditions. *Mar Chem* 103:266–275. <https://doi.org/10.1016/j.marchem.2006.09.005>
- Berg P, Risgaard-Petersen N, Rysgaard S (1998) Interpretation of measured concentration profiles in sediment pore water. *Limnol Oceanogr* 43:1500–1510. <https://doi.org/10.4319/lo.1998.43.7.1500>
- Beulker C, Lessmann D, Nixdorf B (2003) Aspects of phytoplankton succession and spatial distribution in an acidic mining lake (Plessa 117, Germany). *Acta Oecol* 24:25–31. [https://doi.org/10.1016/S1146-609X\(03\)00002-X](https://doi.org/10.1016/S1146-609X(03)00002-X)
- Blodau C (2006) A review of acidity generation and consumption in acidic coal mine lakes and their watersheds. *Sci Total Environ* 369:307–332. <https://doi.org/10.1016/j.scitotenv.2006.05.004>
- Borch T, Kretzschmar R, Skappeler A et al (2010) Biogeochemical redox processes and their impact on contaminant dynamics. *Environ Sci Technol* 44:15–23. <https://doi.org/10.1021/es9026248>
- Bower CE, Holm-Hansen T (1980) A salicylate-hypochlorite method for determining ammonia in seawater. *J Fish Aquat Sci* 37:794–798
- Burger DF, Hamilton DP, Pilditch CA, Gibbs MM (2007) Benthic nutrient fluxes in a eutrophic, polymictic lake. *Hydrobiologia* 584:13–25. <https://doi.org/10.1007/s10750-007-0582-0>
- Cai WJ, Reimers CE (1995) Benthic oxygen flux, bottom water oxygen concentration and core top organic carbon content in the deep northeast Pacific Ocean. *Deep Res Part I* 42:1681–1699. [https://doi.org/10.1016/0967-0637\(95\)00073-F](https://doi.org/10.1016/0967-0637(95)00073-F)
- Canavan RW, Slomp CP, Jourabchi P et al (2006) Organic matter mineralization in sediment of a coastal freshwater lake and response to salinization. *Geochim Cosmochim Acta* 70:2836–2855. <https://doi.org/10.1016/j.gca.2006.03.012>
- Cánovas CR, Ollás M, Macías F et al (2016) Water acidification trends in a reservoir of the Iberian Pyrite Belt (SW Spain). *Sci Total Environ* 541:400–411. <https://doi.org/10.1016/j.scitotenv.2015.09.070>
- Carignan R (1985) Quantitative importance of alkalinity flux from the sediments of acid lakes. *Nature* 314:92–94. <https://doi.org/10.1038/314141a0>
- Clément J-C, Shrestha J, Ehrenfeld JG, Jaffé PR (2005) Ammonium oxidation coupled to dissimilatory reduction of iron under anaerobic conditions in wetland soils. *Soil Biol Biochem* 37:2323–2328. <https://doi.org/10.1016/j.soilbio.2005.03.027>
- Corzo A, Luzon A, Mayayo M et al (2005) Carbonate mineralogy along a biogeochemical gradient in recent lacustrine sediments of Gallocanta Lake (Spain). *Geomicrobiol J* 22:283–298. <https://doi.org/10.1080/01490450500183654>
- Dillon JG, Fishbain S, Miller SR, Bebout BM, Habicht KS, Webb SM, Stahl DA (2007) High rates of sulfate reduction in a low-sulfate hot spring microbial mat are driven by a low level of diversity of sulfate-respiring microorganisms. *Appl Environ Microbiol*. <https://doi.org/10.1128/AEM.00357-07>
- Eglinton TI (2012) Geochemistry: a rusty carbon sink. *Nature* 483:165–166. <https://doi.org/10.1038/483165a>
- Elberling B, Damgaard LR (2001) Microscale measurements of oxygen diffusion and consumption in subaqueous sulfide tailings. *Geochim Cosmochim Acta* 65:1897–1905. [https://doi.org/10.1016/S0016-7037\(01\)00574-9](https://doi.org/10.1016/S0016-7037(01)00574-9)

- Freeman C, Ostle N, Kang H (2001) An enzymic “latch” on a global carbon store. *Nature* 409:149. <https://doi.org/10.1038/35051650>
- Frindte K, Eckert W, Attermeyer K, Grossart HP (2013) Internal wave-induced redox shifts affect biogeochemistry and microbial activity in sediments: a simulation experiment. *Biogeochemistry* 113:423–434. <https://doi.org/10.1007/s10533-012-9769-1>
- Frindte K, Allgaier M, Grossart HP, Eckert W (2016) Redox stability regulates community structure of active microbes at the sediment-water interface. *Environ Microbiol Rep* 8:798–804. <https://doi.org/10.1111/1758-2229.12441>
- Froelich PN, Klinkhammer GP, Bender ML et al (1978) Early oxidation of organic matter in pelagic sediments of the eastern equatorial Atlantic: suboxic diagenesis. *Geochim Cosmochim Acta* 43:1075–1090. [https://doi.org/10.1016/0016-7037\(79\)90095-4](https://doi.org/10.1016/0016-7037(79)90095-4)
- García-Robledo E, Corzo A, Papaspyrou S (2014) A fast and direct spectrophotometric method for the sequential determination of nitrate and nitrite at low concentrations in small volumes. *Mar Chem* 162:30–36. <https://doi.org/10.1016/j.marchem.2014.03.002>
- Geller W, Koschorreck M, Wendt-Potthoff K et al (2009) A pilot-scale field experiment for the microbial neutralization of a holomictic acidic pit lake. *J Geochem Explor* 100:153–159. <https://doi.org/10.1016/j.gexplo.2008.04.003>
- Glud RN (2008) Oxygen dynamics of marine sediments. *Mar Biol Res* 4:243–289. <https://doi.org/10.1080/17451000801888726>
- Grasshoff K, Kremling K, Ehrhardt M (1999) *Methods of seawater analysis*, 3rd edn. Wiley, Weinheim
- Gu B, Schmitt J, Chen Z et al (1995) Adsorption and desorption of different organic matter fractions on iron oxide. *Geochim Cosmochim Acta* 59:219–229. [https://doi.org/10.1016/0016-7037\(94\)00282-Q](https://doi.org/10.1016/0016-7037(94)00282-Q)
- Gunnars A, Blomqvist S (1997) Phosphate exchange across the sediment-water interface when shifting from anoxic to oxic conditions—an experimental comparison of freshwater and brackish-marine systems. *Biogeochemistry* 37:203–226. <https://doi.org/10.1023/A:1005744610602>
- Holmer M, Storkholm P (2001) Sulphate reduction and sulphur cycling in lake sediments: a review. *Freshw Biol* 46:431–451. <https://doi.org/10.1046/j.1365-2427.2001.00687.x>
- Huang S, Jaffé PR (2015) Characterization of incubation experiments and development of an enrichment culture capable of ammonium oxidation under iron reducing conditions. *Biogeosciences* 12:769–779. <https://doi.org/10.5194/bgd-11-12295-2014>
- Hupfer M, Lewandowski J (2008) Oxygen controls the phosphorus release from lake sediments—a long-lasting paradigm in limnology. *Int Rev Hydrobiol* 93:415–432. <https://doi.org/10.1002/iroh.200711054>
- Jeschke C, Falagán C, Knöller K et al (2013) No nitrification in lakes below pH 3. *Environ Sci Technol* 47:14018–14023. <https://doi.org/10.1021/es402179v>
- Jørgensen BB, Bak FB (1991) Pathways and microbiology of thiosulphate transformations and sulfate reduction in a marine sediment (Kattegat, Denmark). *Appl Environ Microbiol* 57:847–856
- Jørgensen BB, Revsbech NP (1983) Colorless sulfur bacteria, *Beggiatoa* spp. and *Thiovulum* spp., in O<sub>2</sub> and H<sub>2</sub>S microgradients. *Appl Environ Microbiol* 45:1261–1270. [https://doi.org/10.1007/978-3-642-30141-4\\_78](https://doi.org/10.1007/978-3-642-30141-4_78)
- Jørgensen BB, Weber A, Zopfi J (2001) Sulfate reduction and anaerobic methane oxidation in Black Sea sediments. *Deep Sea Res Part I* 48:2097–2120. [https://doi.org/10.1016/S0967-0637\(01\)00007-3](https://doi.org/10.1016/S0967-0637(01)00007-3)
- Jost G, Martens-Habben W, Pollehne F et al (2010) Anaerobic sulfur oxidation in the absence of nitrate dominates microbial chemoautotrophy beneath the pelagic chemocline of the eastern Gotland Basin, Baltic Sea. *FEMS Microbiol Ecol* 71:226–236. <https://doi.org/10.1111/j.1574-6941.2009.00798.x>
- Jourabchi P, Van Cappellen P, Regnier P (2005) Quantitative interpretation of pH distributions in aquatic sediments: a reaction-transport modeling approach. *Am J Sci* 305:919–956. <https://doi.org/10.2475/ajs.305.9.919>
- Karimian N, Johnston SG, Burton ED (2017) Effect of cyclic redox oscillations on water quality in freshwater acid sulfate soil wetlands. *Sci Total Environ* 581–582(2017):314–327. <https://doi.org/10.1016/j.scitotenv.2016.12.131>
- Kemp ALW, Thomas RL, Wong HKT, Johnston LM (1977) Nitrogen and C/N ratios in the sediments of Lakes Superior, Huron, St. Clair, Erie, and Ontario. *Can J Earth Sci* 14:2402–2413. <https://doi.org/10.1139/e77-205>
- Kirby CS, Cravotta CA III (2005) Net alkalinity and net acidity 1: theoretical considerations. *Appl Geochem* 20:1920–1940. <https://doi.org/10.1016/j.apgeochem.2005.07.003>
- Kling GW, Giblin AE, Fry B, Peterson BJ (1991) The role of seasonal turnover in lake alkalinity dynamics. *Limnol Oceanogr* 36:106–122. <https://doi.org/10.4319/lo.1991.36.1.0106>
- Koschorreck M (2008) Microbial sulphate reduction at a low pH. *FEMS Microbiol Ecol* 64:329–342. <https://doi.org/10.1111/j.1574-6941.2008.00482.x>
- Koschorreck M, Wendt-Potthoff K, Geller W (2003) Microbial sulfate reduction at low pH in sediments of an acidic lake in Argentina. *Environ Sci Technol* 37:1159–1162. <https://doi.org/10.1021/es0259584>
- Koschorreck M, Bozau E, Frömmichen R et al (2007a) Processes at the sediment water interface after addition of organic matter and lime to an Acid Mine Pit Lake mesocosm. *Environ Sci Technol* 41:1608–1614. <https://doi.org/10.1021/es0614823>
- Koschorreck M, Kleeberg A, Herzsprung P, Wendt-Potthoff K (2007b) Effects of benthic filamentous algae on the sediment-water interface in an acidic mining lake. *Hydrobiologia* 592:387–397. <https://doi.org/10.1007/s10750-007-0776-5>
- Kühl M, Jørgensen BB, Kuhl M, Jørgensen BOB (1992) Reduction and sulfide oxidation in compact microsensor measurements of sulfate reduction and sulfide oxidation in compact microbial communities of aerobic biofilms. *Appl Environ Microbiol* 58:1164–1174
- Kühl M, Steuckart C, Eickert G, Jeroschewski P (1998) A H<sub>2</sub>S microsensor for profiling biofilms and sediments: application in an acidic lake sediment. *Aquat Microb Ecol* 15:201–209. <https://doi.org/10.3354/ame015201>
- Küsel K (2003) Mining lake sediments. *Water Air Soil Pollut* 3:67–90



- Kuwabara JS, Topping BR, Lynch DD et al (2009) Benthic nutrient sources to hypereutrophic upper Klamath Lake, Oregon, USA. *Environ Toxicol Chem* 28:516. <https://doi.org/10.1897/08-207.1>
- Lagauzère S, Moreira S, Koschorreck M (2011) Influence of bioturbation on the biogeochemistry of littoral sediments of an acidic post-mining pit lake. *Biogeosciences* 8:339–352. <https://doi.org/10.5194/bg-8-339-2011>
- Lalonde K, Mucci A, Ouellet A, Gélinas Y (2012) Preservation of organic matter in sediments promoted by iron. *Nature* 483:198–200. <https://doi.org/10.1038/nature10855>
- Lorke A, Muller B, Maerki M, Wuest A (2003) Breathing sediments: the control of diffusive transport across the sediment-water interface by peroxidic boundary-layer turbulence. *Limnol Oceanogr* 48:2077–2085. <https://doi.org/10.4319/lo.2003.48.6.2077>
- Mackin JE, Aller RC (1984) Ammonium adsorption in marine sediments. *Limnol Oceanogr* 29:250–257
- Maerki M, Müller B, Dinkel C, Wehrli B (2009) Mineralization pathways in lake sediments with different oxygen and organic carbon supply. *Limnol Oceanogr* 54:428–438. <https://doi.org/10.4319/lo.2009.54.2.0428>
- Matzinger A, Müller B, Niederhauser P et al (2010) Hypolimnetic oxygen consumption by sediment-based reduced substances in former eutrophic lakes. *Limnol Oceanogr* 55:2073–2084. <https://doi.org/10.4319/lo.2010.55.5.2073>
- Meier J, Babenzien H-D, Wendt-Potthoff K (2004) Microbial cycling of iron and sulfur in acidic coal mining lake sediments. *Biogeochemistry* 67:135–156. <https://doi.org/10.1023/A:1022103419928>
- Meyers PA, Ishiwatari R (1993) Lacustrine organic geochemistry—an overview of indicators of organic matter sources and diagenesis in lake sediments. *Org Geochem* 20:867–900. [https://doi.org/10.1016/0146-6380\(93\)90100-P](https://doi.org/10.1016/0146-6380(93)90100-P)
- Millero FJ, Plese T, Fernandez M (1988) The dissociation of hydrogen sulfide in seawater. *Limnol Oceanogr* 33:269–274. <https://doi.org/10.4319/lo.1988.33.2.0269>
- Morse JW, Morin J (2005) Ammonium interaction with coastal marine sediments: influence of redox conditions on K. *Mar Chem* 95:107–112. <https://doi.org/10.1016/j.marchem.2004.08.008>
- Moser M, Weisse T (2011) The most acidified Austrian lake in comparison to a neutralized mining lake. *Limnologia* 41:303–315. <https://doi.org/10.1016/j.limno.2011.01.002>
- Nixdorf B, Uhlmann W, Lessmann D (2010) Potential for remediation of acidic mining lakes evaluated by hydrochemical modelling: case study Grünewalder Lauch (Plessa 117, Lusatia/Germany). *Limnologia* 40:167–174. <https://doi.org/10.1016/j.limno.2009.12.005>
- Peine A, Tritschler A, Sel KK, Peiffer S (2000) Electron flow in an iron-rich acidic sediment—evidence for an acidity-driven iron cycle. *Limnol Oceanogr* 45:1077–1087. <https://doi.org/10.4319/lo.2000.45.5.1077>
- Rabouille C, Gaillard J (1991) A coupled model representing the deep-sea organic carbon mineralization and oxygen consumption in surficial sediments. *J Geophys Res* 96:2761–2776. <https://doi.org/10.1029/90JC02332>
- Riedel T, Zak D, Biester H, Dittmar T (2013) Iron traps terrestrially derived dissolved organic matter at redox interfaces. *Proc Natl Acad Sci USA* 110:10101–10105. <https://doi.org/10.1073/pnas.1221487110>
- Sánchez-España J, Yusta I, Díez-Ercilla M (2011) Schwertmannite and hydrobasaluminite: a re-evaluation of their solubility and control on the iron and aluminium concentration in acidic pit lakes. *Appl Geochem* 26:1752–1774. <https://doi.org/10.1016/j.apgeochem.2011.06.020>
- Sarmiento AM, Ollás M, Nieto JM et al (2009) Natural attenuation processes in two water reservoirs receiving acid mine drainage. *Sci Total Environ* 407:2051–2062. <https://doi.org/10.1016/j.scitotenv.2008.11.011>
- Schweifel R, Steinsberger T, Bouffard D et al (2017) Using small-scale measurements to estimate hypolimnetic oxygen depletion in a deep lake. *Limnol Oceanogr*. <https://doi.org/10.1002/lno.10723>
- Sinninghe Damste JS, De Leeuw JW (1990) Analysis, structure and geochemical significance of organically-bound sulphur in the geosphere: state of the art and future research. *Org Geochem* 16:1077–1101. [https://doi.org/10.1016/0146-6380\(90\)90145-P](https://doi.org/10.1016/0146-6380(90)90145-P)
- Skoog AC, Arias-Esquivel VA (2009) The effect of induced anoxia and reoxygenation on benthic fluxes of organic carbon, phosphate, iron, and manganese. *Sci Total Environ* 407:6085–6092. <https://doi.org/10.1016/j.scitotenv.2009.08.030>
- Smith J, Melville MD (2004) Iron monosulfide formation and oxidation in drain-bottom sediments of an acid sulfate soil environment. *Appl Geochem* 19:1837–1853. <https://doi.org/10.1016/j.apgeochem.2004.04.004>
- Soetaert K, Hofmann AF, Middelburg JJ et al (2007) The effect of biogeochemical processes on pH. *Mar Chem* 105:30–51. <https://doi.org/10.1016/j.marchem.2007.06.008>
- Soetaert K, Petzoldt T, Meysman F (2010) Marelac: tools for aquatic sciences. R package. <http://CRAN.R-project.org/package=marelac>
- Sweerts J-PRA, Bär-Gilissen M-J, Cornelese AA, Cappenberg TE (1991) Oxygen-consuming processes at the profundal and littoral sediment-water interface of a small meso-eutrophic lake (Lake Vechten, The Netherlands). *Limnol Oceanogr* 36:1124–1133. <https://doi.org/10.4319/lo.1991.36.6.1124>
- Thamdrup B (2012) New pathways and processes in the global nitrogen cycle. *Annu Rev Ecol Evol Syst* 43:407–428. <https://doi.org/10.1146/annurev-ecolsys-102710-145048>
- Torres E, Ayora C, Cánovas CR et al (2013) Metal cycling during sediment early diagenesis in a water reservoir affected by acid mine drainage. *Sci Total Environ* 461–462:416–429. <https://doi.org/10.1016/j.scitotenv.2013.05.014>
- Torres E, Ayora C, Jiménez-Arias JL et al (2014) Benthic metal fluxes and sediment diagenesis in a water reservoir affected by acid mine drainage: a laboratory experiment and reactive transport modeling. *Geochim Cosmochim Acta* 139:344–361. <https://doi.org/10.1016/j.gca.2014.04.013>
- Torres E, Galván L, Cánovas CR et al (2016) Oxycline formation induced by Fe(II) oxidation in a water reservoir affected by acid mine drainage modeled using a 2D hydrodynamic and water quality model—CE-QUAL-W2. *Sci Total Environ* 562:1–12. <https://doi.org/10.1016/j.scitotenv.2016.03.209>

- Totsche O, Pöthig R, Uhlmann W et al (2003) Buffering mechanisms in acidic mining lakes—a model-based analysis. *Aquat Geochem* 9:343–359. <https://doi.org/10.1023/B:AQUA.0000029035.88090.eb>
- Urban NR, Brezonik PL, Baker LA, Sherman LA (1994) Sulfate reduction and diffusion in sediments of Little Rock Lake, Wisconsin. *Limnol Oceanogr* 39:797–815. <https://doi.org/10.4319/lo.1994.39.4.0797>
- Wendt-Potthoff K, Koschorreck M (2002) Functional groups and activities of bacteria in a highly acidic volcanic mountain stream and lake in Patagonia, Argentina. *Microb Ecol* 43:92–106. <https://doi.org/10.1007/s00248-001-1030-8>
- Wendt-Potthoff K, Koschorreck M, Diez Ercilla M, Sánchez España J (2012) Microbial activity and biogeochemical cycling in a nutrient-rich meromictic acid pit lake. *Limnologica* 42:175–188. <https://doi.org/10.1016/j.limno.2011.10.004>
- Yang WH, Weber KA, Silver WL (2012) Nitrogen loss from soil through anaerobic ammonium oxidation coupled to iron reduction. *Nat Geosci* 5:538–541. <https://doi.org/10.1038/ngeo1530>
- Zonneveld KAF, Versteegh GJM, Kasten S et al (2010) Selective preservation of organic matter in marine environments; processes and impact on the sedimentary record. *Biogeosciences* 7:483–511. <https://doi.org/10.5194/bg-7-483-2010>